Available online at www.sciencedirect.com
ScienceDirect
Journal of the European Ceramic Society 28 (2008) 2309–2317
www.elsevier.com/locate/jeurceramsoc

# Residual stresses in YAG phase of melt growth $Al_2O_3$/YAG eutectic composite estimated by indentation fracture test and finite element analysis

S. Ochiai [a,*], S. Ikeda [b], S. Iwamoto [b], J.J. Sha [a], H. Okuda [a], Y. Waku [c], N. Nakagawa [c], A. Mitani [c], M. Sato [c], T. Ishikawa [c]

[a] *International Innovation Center, Kyoto University, Yoshida, Sakyo-ku, Kyoto 606-8501, Japan*
[b] *Graduate School of Engineering, Kyoto University, Sakyo-ku, Kyoto 606-8501, Japan*
[c] *Ube Research Laboratory, Corporate Research & Development, UBE Industries Ltd., Ube City, Yamaguchi 755, Japan*

Available online 4 March 2008

**Abstract**

The residual stresses in YAG phase of the melt growth $Al_2O_3$/YAG eutectic composite were studied at room temperature by means of the indentation fracture test and finite element stress analysis. The YAG phase taken out from the composite was used as a reference sample without thermally induced residual stresses. The apparent fracture toughness of YAG phase with residual stress in the composite was higher than that of the reference sample of bare YAG. From the difference in fracture toughness value between the YAG in the composite and the bare YAG, the residual stress of YAG in the composite was estimated to be $-170 \pm 100$ and $-220 \pm 130$ MPa in the cross-sections perpendicular and parallel to the solidification direction, respectively. The experimentally measured spatial distribution of the residual stress in YAG phase in the composite was accounted for by the result of finite element analysis, which showed that the residual stress is different from position to position due to the variation in local morphology of YAG and $Al_2O_3$ within the composite.


*Keywords:* Composites; Mechanical properties; $Al_2O_3$/YAG

## 1. Introduction

Considerable efforts have been made to develop high performance materials with excellent high-temperature strength to improve thermal efficiency in jet aircraft engines and high efficiency power-generation gas turbines. Among the developed materials, the unidirectionally solidified eutectic ceramic composites have clean interface, high-thermo-dynamical compatibility between/among the constituting phases and high static and creep strengths,[1–15] being attractive and promising for structural application. For application of these composite materials to industrial products such as gas turbine components, the study on mechanical behavior at room temperature is also important since these materials will be handled to fabricate machine components at room temperature. For analysis of mechanical behavior at room temperature, it is demanded to estimate the residual stresses introduced during cooling from solidification- to room temperature.

In the $Al_2O_3$/YAG composite, as the coefficient of thermal expansion of YAG is close to that of $Al_2O_3$,[15–17] the thermally induced stresses are low in comparison with the other directionally solidified eutectic composites, as has been reported by Llorca and Orera,[15] Dickey et al.[17] and Torii et al.[18] In the present work, it was attempted to elucidate the residual stress value and its distribution in detail. The outline of the contents of this paper is as follows.

(1) In order to obtain the reference sample without thermally induced residual stress, the bare YAG was taken out from the $Al_2O_3$/YAG composite by removing $Al_2O_3$, as shown in Section 2.1. From the difference in fracture toughness between the YAG in the composite and bare YAG, the residual stress of YAG in the composite was estimated. As the fracture toughness of YAG was low as will be shown later in Section 3.2, the apparent fracture toughness was strongly affected by the existent residual stress, making it possible to detect the residual stress in YAG, even though the stress level was low.
(2) From the difference in fracture toughness between the YAG in the composite and bare YAG phase, the average residual

* Corresponding author. Tel.: +81 75 753 4834; fax: +81 75 753 4841.
*E-mail address:* ochiai@iic.kyoto-u.ac.jp (S. Ochiai).

0955-2219/$ – see front matter © 2008 Elsevier Ltd. All rights reserved.
doi:10.1016/j.jeurceramsoc.2008.01.013

stress in YAG in the composite was estimated to be around −220 to −170 MPa as shown in Section 3.3. Such a result was described well by the finite element analysis, which showed around −180 to −150 MPa. In addition to the indentation fracture test and finite element analysis employed in the present work, the X-ray diffraction method was also employed to measure the residual stress for the same composite and reference samples, whose result is submitted in a separated paper.[19] It is noted that the average residual stress estimated by the X-ray method was around −220 to −160 MPa, being comparable to the result of the present work.

(3) The fracture toughness- and residual stress values in YAG in the composite were widely distributed, as shown in Sections 3.2 and 3.3. The reason for this was accounted for by the result of the finite element analysis from the viewpoint of the widely distributed residual stress stemming from the variation in local morphology of YAG and $Al_2O_3$ within the composite, as will be shown in Section 3.4.

## 2. Experimental procedure

### 2.1. Sample

High purity α-$Al_2O_3$ and $Y_2O_3$ powders with a eutectic mole ratio of 82:18 were ball-milled in ethanol. Thus obtained slurry was dried and pre-melt by arc-melting to obtain initial ingots. The ingots were crushed and the powders were melted in a Mo crucible by high frequency induction heating at a pressure of $1.3 \times 10^{-3}$ Pa in an argon atmosphere. After sustaining the melt at 2223 K for 1.8 ks, the melt was solidified unidirectionally by descending the Mo crucible at a speed of $1.39 \times 10^{-6}$ m/s. The volume fraction of $Al_2O_3$ and YAG in the fabricated composite was 0.5 for each.[3]

In the present work, the residual stress was measured from the difference in fracture toughness between the YAG in the composite with thermally induced residual stress and the bare YAG without it by the procedure shown later in Section 2.4. The bare YAG was obtained by removing $Al_2O_3$ from the $Al_2O_3$/YAG composite by deoxidization of $Al_2O_3$ in carbon container in vacuum at 1873 K for 7.2 ks. Under this deoxidization condition, the depth of the $Al_2O_3$-removed region in the thickness direction of the sample was around 250 μm, being around 8–25 times the thickness of the YAG (around 10–30 μm). The appearance of the surface of thus prepared bare YAG sample is presented in Fig. 1.

### 2.2. Observation of propagation process of cracks induced by high load indentation

Fig. 2 shows the schematic representation of the relation of crack propagation path in relation to residual stresses, focusing on the curved parts. As shown later, the residual stress in YAG was compressive. This means that the coefficient of thermal expansion of α(YAG) is lower than that of α($Al_2O_3$). Under such a condition, the following crack path is expected. When the crack existing in $Al_2O_3$ approaches the YAG, the crack extends into YAG due to the tensile circumferential residual stress of

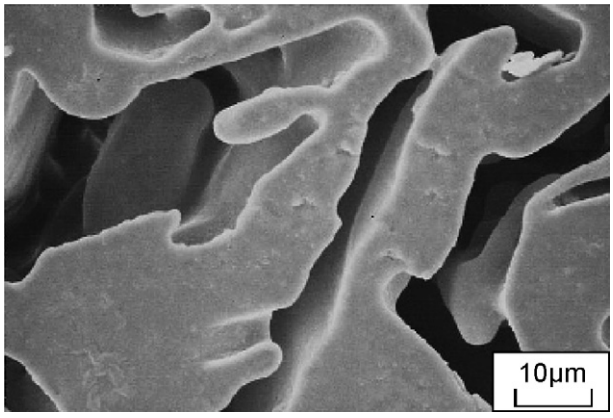


Fig. 1. Appearance of the bare YAG, prepared by removing $Al_2O_3$ from the $Al_2O_3$/YAG composite.

$Al_2O_3$ as in Fig. 2(a). On the other hand, when the crack existing in YAG approaches $Al_2O_3$, the crack by-passes $Al_2O_3$ due to the tensile radial residual stress at interface as in Fig. 2(b). While YAG and $Al_2O_3$ are not particles in the present composite, such features will be observed at least for the parts where the YAG and $Al_2O_3$ are curved in shape. Thus, from the observation of the crack process, which of YAG and $Al_2O_3$ has compressive residual stress can be identified.

When indentation test is done at appropriate high loads, the crack induced by the indentation propagates by breaking the $Al_2O_3$, YAG and their interfaces alternatively and stops finally. In the present work, the indentation test at a high load of 196 N was carried out with hardness measurement machine (AVK-C1, Akashi Co. Ltd.). Then the crack propagation process, covering around 10–20 phases of $Al_2O_3$ and YAG in the cross-section, was observed with SEM (scanning electron microscope) (JSM-5410LS, Jeol Co. Ltd.) to examine whether the expected features occur in the present composite or not. The result is presented in Section 3.1.

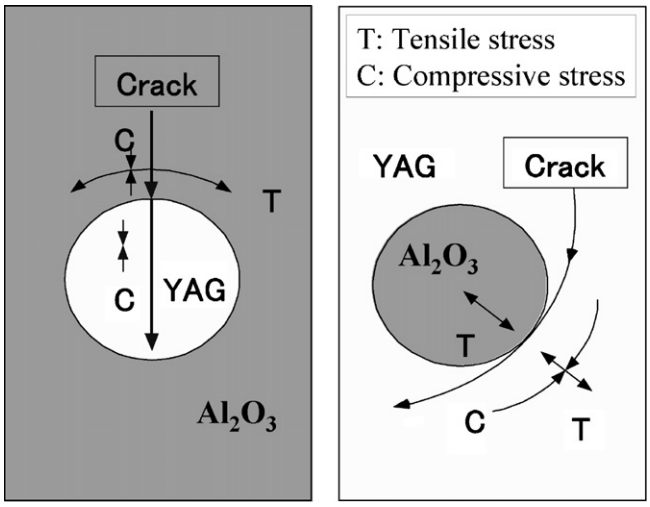


Fig. 2. Local stress field caused by cooling due to the difference in coefficient of thermal expansion between YAG and $Al_2O_3$ phases and its influence on crack propagation under the condition where the coefficient of thermal expansion of YAG is lower than that of $Al_2O_3$.

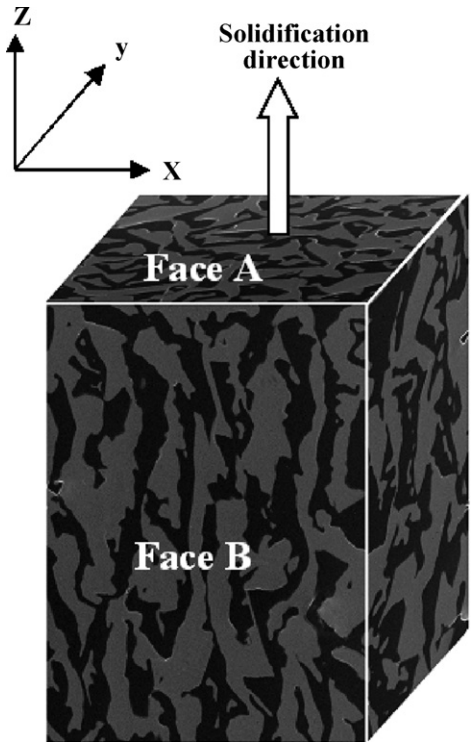


Fig. 3. The morphology of Faces A and B, perpendicular and parallel to the solidification direction, respectively, on which indentation test was carried out.

### 2.3. Indentation fracture test

The indentation fracture test (IF test) was carried out using dynamic micro-hardness machine (HMV-2000, Shimadzu Co. Ltd.) at a load 0.49 N with a holding time 10 s, for Faces A and B, which are perpendicular and parallel to the solidification direction, respectively, as shown in Fig. 3. For convenience, we define $x$, $y$ and $z$ directions as in Fig. 3. Faces A and B correspond to $x$–$y$ and $x$–$z$ planes, respectively. The sizes of the indentation and induced crack were measured with SEM.

Until now, two empirical equations have been proposed to estimate fracture toughness from the IF test; Evans's equation for median crack[20] and Niihara's one for palmqvist crack.[21] In order to know which equation is applicable to the present samples, the indented sample was broken by bending and the appearance of the indentation-induced crack beneath the indentation (Fig. 4) was observed with SEM. The hatched cross-section in Fig. 4 corresponds to fracture surface by bending. From the observed morphology of the cracks beneath the indentation, it was identified which median and palmqvist cracks were induced by the indentation. Based on such a result, the corresponding equation was used for estimation of the fracture toughness values. The result will be presented in Section 3.2.

### 2.4. Estimation of residual stress

For the materials with residual stresses, the fracture toughness $K_{Ic}$ is a function of the crack size $c$ and the residual stress $\sigma_R$.[22] Noting the fracture toughness under no residual stress as $K^*_{Ic}$,

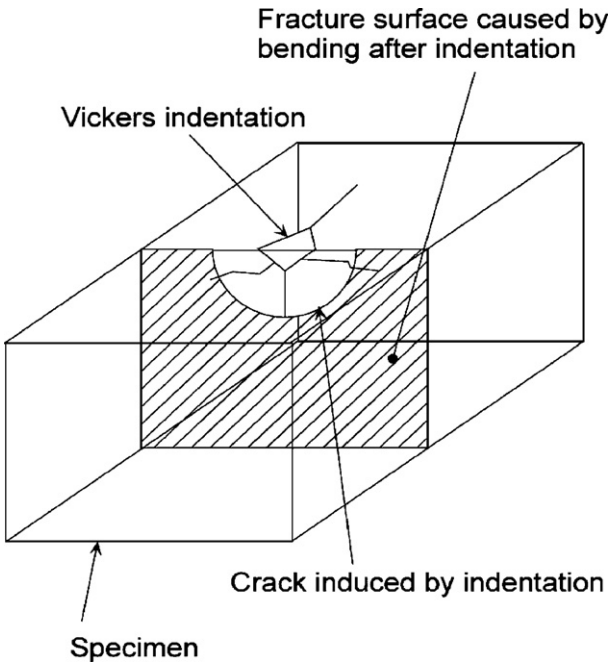


Fig. 4. Schematic representation of the indentation-induced crack, whose morphology beneath the indentation was observed from the fracture surface caused by bending after indentation.

the relation among the $K_{Ic}$, $K^*_{Ic}$, $c$ and $\sigma_R$ is expressed by[22,23]

$$K_{Ic} = K^*_{Ic} - 2\sigma_R\left(\frac{c}{\pi}\right)^{1/2} \quad (1)$$

Substituting the measured values of $K_{Ic}$ and $c$ of YAG in composite, and $K^*_{Ic}$ of bare YAG into Eq. (1), $\sigma_R$ was calculated. The result will be shown in Section 3.3.

### 2.5. Finite element analysis

The Young's modulus values of the $Al_2O_3$/YAG composite at room temperature for the directions parallel, 45°—inclined and perpendicular to the solidification direction have been reported to be 333, 329 and 342 GPa, respectively,[16] indicating that the anisotropy (difference in Young's modulus among the directions) is small for the Young's modulus. Also, in the measured coefficient of thermal expansions for the directions parallel, 45°, perpendicular to the solidification direction, the anisotropy was small as well as for Young's modulus, as shown in Fig. 5.[16] It was attempted in our former work[16] to describe such measured temperature-dependences of the Young's modulus and coefficient of thermal expansion of the composite by the finite element method (FEM). Various reported temperature-dependences of Young's modulus and coefficient of thermal expansion for single crystal YAG and $Al_2O_3$ were input for calculation. However, within the reported data for single crystals, reasonable calculation results, satisfying simultaneously the measured temperature-dependences of Young's modulus and coefficient of thermal expansion of the composite for the three directions, could not be found. Then, as a first approximation, the following temperature ($T$) dependence of Young's modulus ($E$) and coefficient of thermal expansion ($\alpha$) of polycrystalline

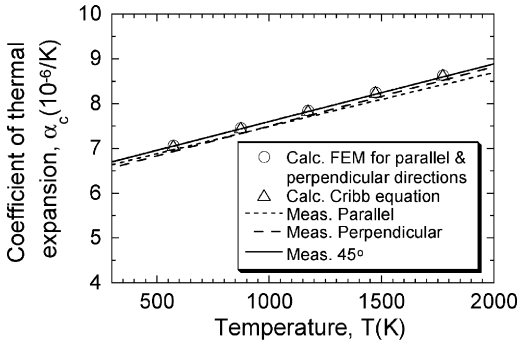


Fig. 5. Comparison of the temperature dependence of the coefficient of thermal expansion of the composite for parallel ($z$ direction in Fig. 3) and perpendicular ($x$ and $y$ directions) directions calculated by the finite element method (FEM) and that calculated by the Cribb equation with the measured ones for parallel, perpendicular and 45° directions. As the difference in temperature dependence of the coefficient of thermal expansion calculated by FEM between the parallel and perpendicular directions was too small to be distinguished in the present scale, the calculation results for both directions are shown with the same symbol (◯). The result calculated by Cribb equation (△) is dependent only of volume fraction, giving the same result for any direction.

$Al_2O_3$ and YAG[24–27] were input.

$$E(Al_2O_3) = 423 - 0.0474T \ \text{(GPa)}, \quad (2)$$

$$E(\text{YAG}) = 299 - 0.0180T \ \text{(GPa)}, \quad (3)$$

$$\alpha(Al_2O_3) = 6.50 + 0.00146T \ (\times 10^{-6}\,\text{K}^{-1}), \quad (4)$$

$$\alpha(\text{YAG}) = 6.09 + 0.00117T \ (\times 10^{-6}\,\text{K}^{-1}) \quad (5)$$

The calculation result for the temperature dependence of the coefficient of thermal expansion of the composite is presented in Fig. 5. As the difference in calculated temperature dependence of the coefficient of thermal expansion of the composite for the parallel ($z$ direction in Fig. 3) and perpendicular ($y$ direction) was too small to be distinguished in the present scale, the calculation results for both directions are shown with the same symbol (◯). For reference, the result calculated by Cribb equation,[28] which gives the same result for any direction when isotropic values are input, is also presented with △. The calculation results were close to the experimental ones. In this way, when Eqs. (2)–(5) taken from the reported data for polycrystalline were used, the experimentally measured temperature dependence of the thermal expansion of the composite could be described fairly well by the finite element analysis as well as by the Cribb's model.[28]

In the present work, Eqs. (2)–(5) that could give the calculation results close to the measured temperature-dependences of Young's modulus and coefficient of thermal expansion of the composite were used as a first approximation for the finite element analysis to calculate the residual stress distribution in $Al_2O_3$ and YAG. On this point, the present calculation is rough; further study is needed for refinement. It is, however, noted that the present calculation showed that the average residual stress of YAG in composite is around −180 to −150 MPa and the range of residual stress is around −300 to 0 MPa, as shown later. These values are similar to the average values −220 to −170 MPa and the range from −500 to 0 MPa estimated by the indentation fracture test and similar to −220 to −160 MPa estimated by X-ray diffraction.[19] These results suggest that the present input values for calculation are not so much different from the actual ones.

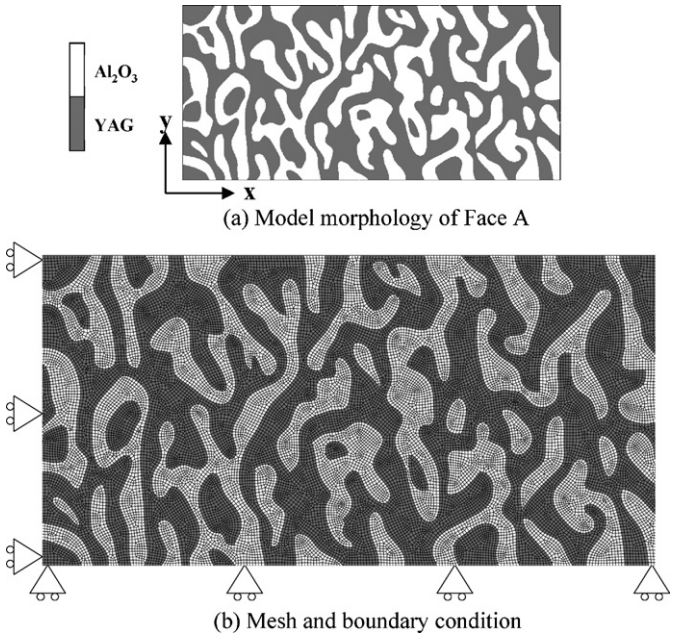


Fig. 6. The finite element model of Face A for analysis of residual stresses. (a) Model morphology of Face A and (b) mesh and boundary condition.

The present finite element analysis was carried with the commercial finite element code MARC/Mentat™. The model morphology of Face A and given meshes is representatively shown in Fig. 6. (The model morphology of Face B will be shown later in Fig. 14(a).) The Poisson's ratio of $Al_2O_3$ and YAG was taken to be 0.23 and 0.25, respectively.[29] For calculation of the residual stresses, it was needed to know the "stress free" temperature, at which the build-up of elastic stresses begins, since the elastic strains generated by the thermal expansion mismatch above this temperature are smoothed out by the plastic or creep deformation of one (or both) phases.[15] In the present calculation, the onset temperature of dislocation slip in prismatic and pyramidal planes in $Al_2O_3$, 1423 K, was taken as the "stress free" temperature, which has been used for analysis of residual stresses in $Al_2O_3$/YSZ composite.[15] The calculation result will be presented in Section 3.4.

## 3. Results and discussion

### 3.1. Crack propagation path

As stated in Section 2.1, it is expected that the crack in the $Al_2O_3$ tends to extend directly into YAG, but the crack in YAG tends to by-pass the $Al_2O_3$ if YAG and $Al_2O_3$ have compressive and tensile residual stresses, respectively. Fig. 7 shows the observed propagation path of the indentation-induced crack. As high load of 196 N was applied in this test, the crack propagated for long distance. The arrows show the direction of the crack propagation. The expected tendency is clearly found, demonstrating that YAG and $Al_2O_3$ have compressive and tensile residual stresses, respectively, and therefore the coefficient

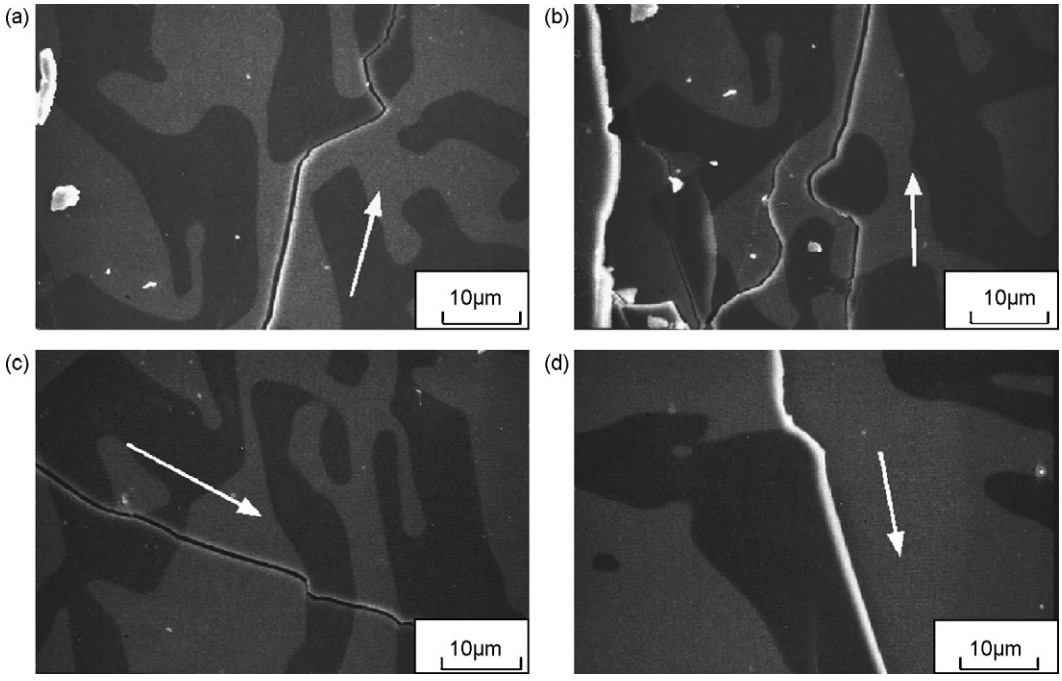


Fig. 7. Examples of the observed propagation path of the crack induced by high load indentation in Face A of $Al_2O_3$/YAG composite.

of thermal expansion of YAG is lower than that of $Al_2O_3$. This result indicates that the apparent fracture toughness of the YAG in composite is higher than that of the bare YAG due to the existent compressive stress.

### 3.2. Fracture toughness of bare YAG and YAG in composite

In order to know which of the Evans's[20] and Niihira's[21] equations is applicable to estimate the fracture toughness, the appearance of the crack beneath the indentation (Fig. 4) was observed. As shown in Fig. 8, the median crack was formed. This indicates that the Evans's equation, which premises the median crack, is applicable to the present YAG. Also the damage zone was formed just beneath the indentation, due to which lateral crack was formed upon unloading process.[30]

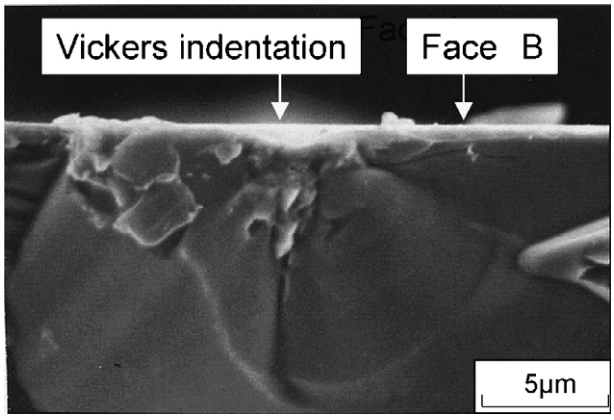


Fig. 8. Appearance of the indentation-induced crack beneath the indented surface, observed in the fracture surface of specimens caused by bending after indentation.

The Vickers indentation-induced crack in YAG is schematically represented as shown in Fig. 9. The Evans's equation[20] is given by

$$K_{\mathrm{Ic}} = 0.036E^{0.4}P^{0.6}a^{-0.7}\left(\frac{c}{a}\right)^{-1.5} \tag{6}$$

where $E$ is the Young's modulus, $2c$ the crack size, $P$ the load and $2a$ the diagonal length. The Young's modulus of YAG at room temperature was taken to be 290 GPa.[16]

Fig. 10 shows the examples of appearance of Vickers indentations in Face A of the YAG in composite and bare YAG. The crack propagated in the diagonal directions. Substituting the

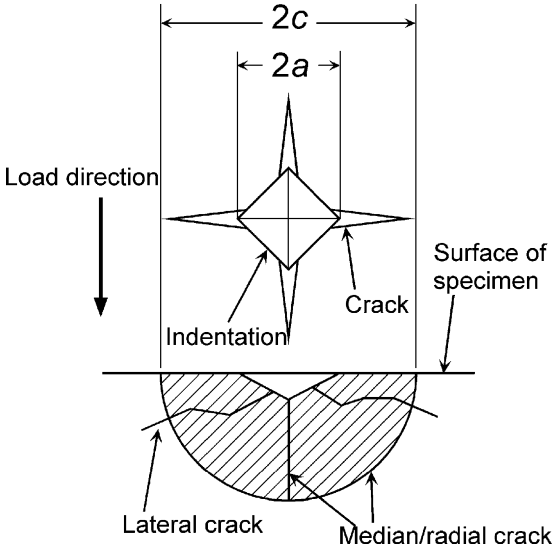


Fig. 9. Schematic representation of Vickers indentation-induced fracture.

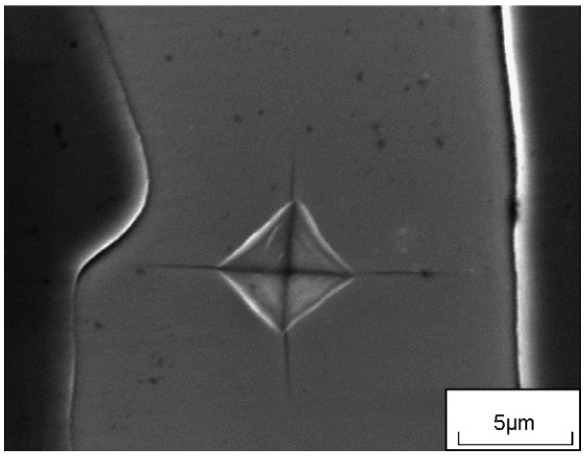


(a) YAG in composite.

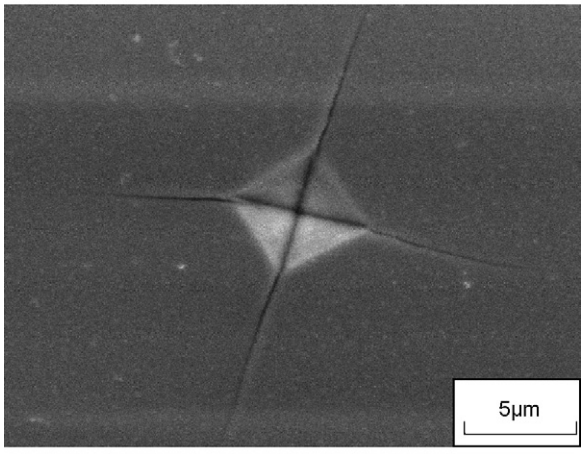


(b) Bare YAG

Fig. 10. Appearance of Vickers indentations in Face A of (a) YAG in the composite and (b) bare YAG.

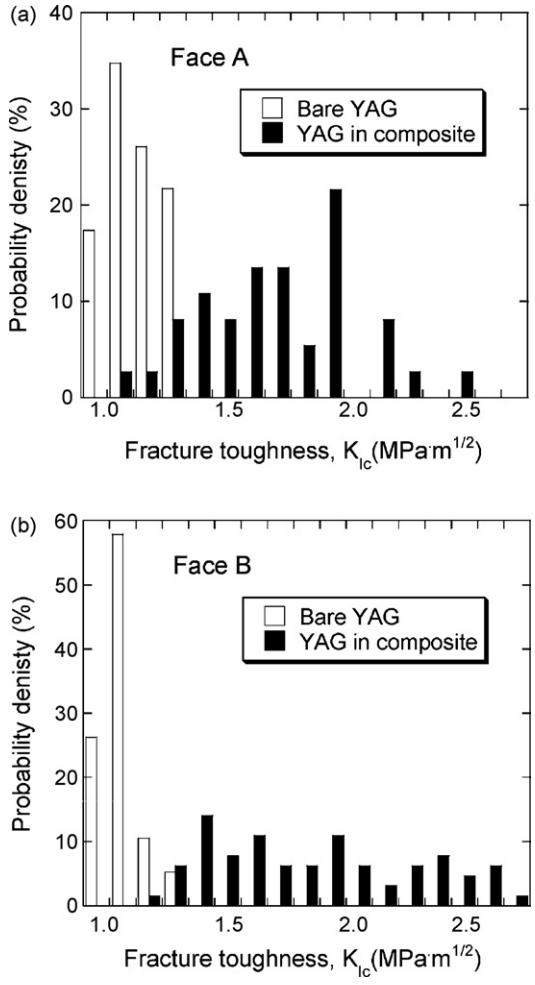


Fig. 11. Measured fracture toughness of YAG in the composite and bare YAG in Faces (a) A and (b) B.

measured $a$ and $c$ values into Eq. (5), the $K_{Ic}^{*}$ and $K_{Ic}$ values were obtained.

$K_{Ic}^{*}$ and $K_{Ic}$ values at more than 30 points were measured for A- and B-faces. The results are shown in Fig. 11. The measured values are numerically expressed as follows:

$$K_{Ic}^{*} = 1.11 \pm 0.09\,\mathrm{MPa\,(m)^{1/2}},$$
$$K_{Ic} = 1.69 \pm 0.30\,\mathrm{MPa\,(m)^{1/2}} \quad \text{for Face A.}$$
$$K_{Ic}^{*} = 1.04 \pm 0.08\,\mathrm{MPa\,(m)^{1/2}},$$
$$K_{Ic} = 1.78 \pm 0.39\,\mathrm{MPa\,(m)^{1/2}} \quad \text{for Face B.}$$

Two distinct features are read. (i) The fracture toughness value of the bare YAG, $K_{Ic}^{*}$, was lower than that of the YAG in composite, $K_{Ic}$, suggesting the existence of the compressive residual stress. (ii) The scatter of fracture toughness $K_{Ic}^{*}$ of the bare YAG was small, while the scatter of fracture toughness $K_{Ic}$ of the YAG in composite was large. The reason for this is attributed to the large scatter of residual strain value of YAG in the composite, which is different from position to position due to the non-uniformity of the local shape and local volume fraction of the constituents ($Al_2O_3$, YAG), as will be discussed in Section 3.4.

### 3.3. Estimation of residual stress in YAG in composite from the $K_{Ic}^{*}$ and $K_{Ic}$

The average fracture toughness values of the bare YAG ($K_{Ic}^{*}$) and YAG ($K_{Ic}$) in composite in Face A were 1.11 and 1.69 MPa (m)$^{1/2}$, respectively, from which the average residual stress $\sigma_R$ was estimated to be −170 MPa by Eq. (1). In a similar manner, from the difference in average $K_{Ic}^{*}$ (1.05 MPa (m)$^{1/2}$) and $K_{Ic}$ (1.78 MPa (m)$^{1/2}$) in Face B, the average residual stress $\sigma_R$ was estimated to be −220 MPa. The existence of the compressive residual stress in YAG and tensile one in $Al_2O_3$ is reconfirmed experimentally by the indentation fracture test as well as by observation of the crack propagation path shown in Section 3.1.

The fracture indentation test showed that the $K_{Ic}$ in the YAG in composite is widely distributed in comparison with the $K_{Ic}^{*}$ of bare YAG (Fig. 11). Such a relatively large distribution of $K_{Ic}$ of the YAG in composite implies the large distribution of the residual stress. In our recent X-ray diffraction experiment,[19] the full width at half maximum intensity of the Bragg peak of the YAG in composite was larger than that of the bare YAG, which also implies the distributed residual stresses. The distribution of the

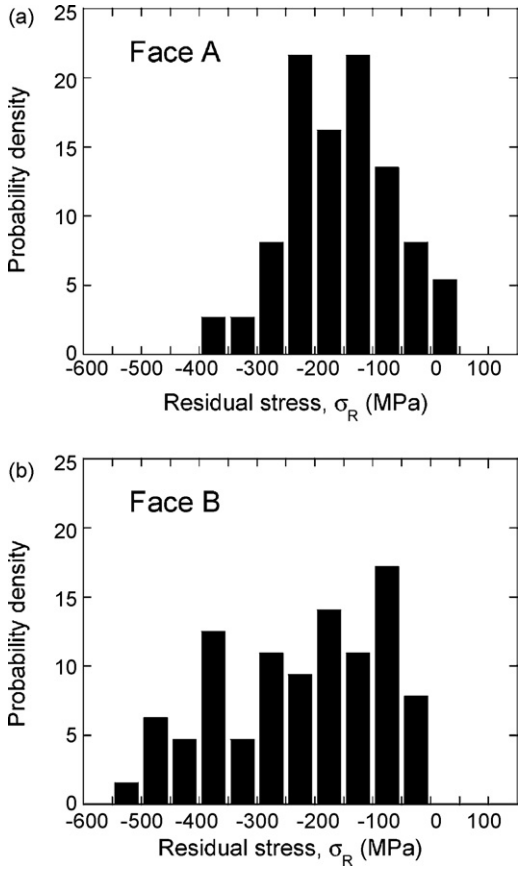


Fig. 12. Residual stress distribution in YAG in composite, estimated by Eq. (1).

residual stress of the YAG in composite was roughly estimated from the distribution of $K_{Ic}$ as follows.

If we assume that the distribution in fracture toughness stems from the difference of the residual stress, we have the residual stress distribution by substituting the measured $K_{Ic}$ and $c$ values into Eq. (1) for each data and average value of $K^*_{Ic} = 1.11$ and 1.05 MPa $(m)^{1/2}$ for Faces A and B, respectively. The result is presented in Fig. 12. In these results, the residual stress varied from −400 to 0 MPa for Face A and from −500 to 0 MPa for Face B. The statistical result of the average stress with the standard deviation for Face A was $-170 \pm 100$ MPa and that for Face B was $-220 \pm 130$ MPa. In this way, the residual stress was widely distributed, depending on the position at which the indentation test was conducted. The present experimentally estimated distribution of the residual stress in YAG will be compared with that calculated by the FEM in Section 3.4.

The compressive residual stress for Face B was slightly higher than that for Face A. Two possible reasons for this difference are anisotropy especially of $Al_2O_3$ and difference in morphology of $Al_2O_3$ and YAG between Faces A and B ($Al_2O_3$ and YAG are elongated along the solidification direction in Face B but not in Face A (Fig. 3)). As the input values for finite element analysis of residual stresses were taken from the reported data for polycrystalline $Al_2O_3$ and YAG (2.5), the influence of their anisotropy on the residual stresses could not be examined within the present work but the influence of the morphology could be examined. In Section 3.4, the influence of the morphology on the average residual stresses will be shown.

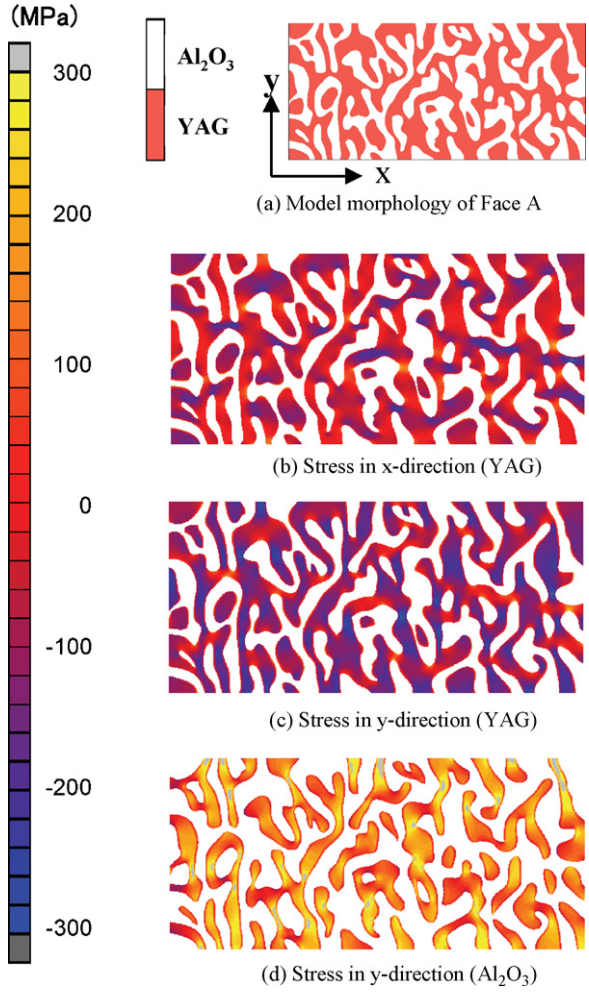


Fig. 13. Residual stress distributions in YAG and $Al_2O_3$ in the composite at room temperature calculated by the finite element method for Face A. (a) Model composite. (b) Residual stress in YAG in the $x$ direction. (c) Residual stress in YAG in the $y$ direction. (d) Residual stress in $Al_2O_3$ in the $y$ direction.

### *3.4. Residual stress distribution in YAG in composite calculated by the FEM*

Fig. 13 shows the residual stress distribution in Face A. The model used for finite element calculation is presented in Fig. 13(a). This model was taken from the observed morphology. The red and white parts correspond to YAG and $Al_2O_3$, respectively. Totally 27,292 elements and 27,595 nodes were given for calculation. Fig. 13(b)–(d) show the stress distributions in YAG in the $x$ direction in Fig. 3, in YAG in the $y$ direction and in $Al_2O_3$ in the $y$ direction, respectively. Fig. 14 shows the residual stress distribution in Face B. The model for Face B was taken also from the observed morphology. Totally 27,312 elements and 27,643 nodes were given for calculation. The calculation result of a part of the model (surrounded with broken lines in Fig. 14(a)) is picked up to show clearly the stress distributions within (b) YAG and (c) $Al_2O_3$ in the $z$ direction. The following features are read from Figs. 13 and 14.

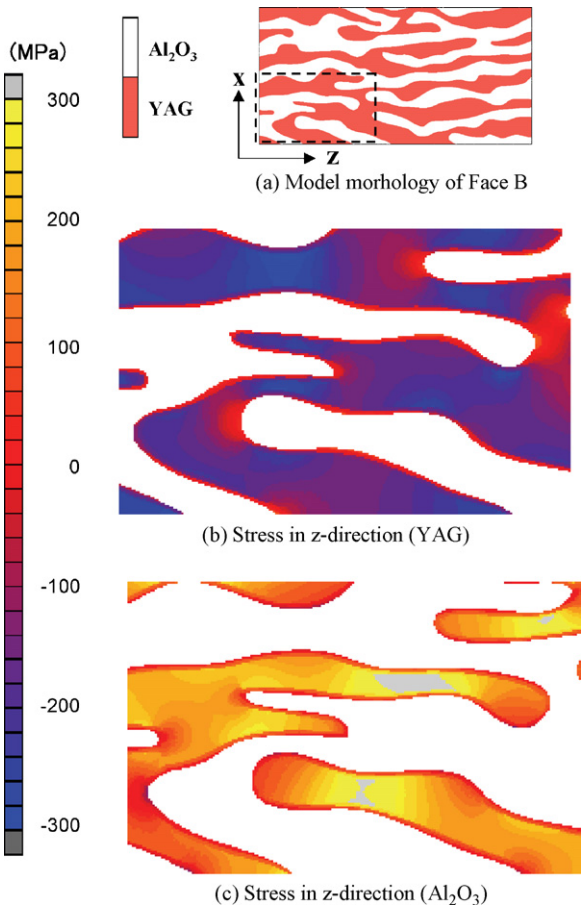


Fig. 14. (a) The model morphology of Face B and examples of the residual stress distribution in the $z$ direction in (b) YAG and (c) $Al_2O_3$ in composite at room temperature, calculated by the finite element method for Face B. The part surround by the broken lines in (a) is representatively picked up and is enlarged to show the detailed residual stress distributions within (b) YAG and (c) $Al_2O_3$.

(1) The $Al_2O_3$ and YAG have tensile and compressive stresses, respectively. The stresses are not uniform, being different from position to position. Also the stresses in $x$, $y$ and $z$ directions are different. In this way, the residual stresses are dependent on the local morphological factors such as thickness, curvature and local volume fraction.
(2) The residual stresses in both YAG and $Al_2O_3$ vary with position (around from −300 to 0 MPa in YAG and around from 0 to 300 MPa in $Al_2O_3$). The calculated residual stress range in YAG was comparable to the measured range from −400 to 0 MPa for Face A and from −500 to 0 MPa for Face B (Fig. 11). The average stress of YAG in Face A ($=(\sigma_x+\sigma_y)/2$) was −150 MPa and that in Face B ($=(\sigma_x+\sigma_z)/2$) was −180 MPa. The difference in the calculated average value between Faces A and B is attributed to the difference in morphology (Fig. 3). These calculated average values were comparable to the average values of −170 and −220 MPa estimated by the indentation fracture test and of −160 and 220 MPa estimated by the X-ray diffraction method,[19] for Faces A and B, respectively.
(3) For calculation of residual stresses, the onset temperature of dislocation slip in prismatic and pyramidal planes in $Al_2O_3$, 1423 K, was taken as the "stress free" temperature as stated in Section 2.5. However, in practice, the "stress free" temperature is not a fixed value, since it is dependent on fabrication condition such as the temperature gradient and cooling rate after solidification. If we take the "stress free" temperature as 1623 K for instance, the average stresses in Faces A and B become −180 and −210 MPa, being closer to the measured values of −170 and −220 MPa, respectively. Namely if the amount of plastic (or creep) deformation is not sufficient to release the accumulated elastic residual strain, the residual stress becomes higher. For calculation of the residual stress, we need exact value of "stress free" temperature, which is unknown until now. It is, however, noted again that the calculated average residual stresses are comparable to the measured values. This suggests that the "stress free" temperature 1423 K practically gives a fairly good approximation for calculation of residual stress distribution. Conclusively, the calculation results in Figs. 13 and 14, showing the wide distribution of the residual stress (around −300 to 0 MPa in YAG and around 0 to +300 MPa in $Al_2O_3$), are considered not to be so much different from the practical ones. The residual stress is different from position to position, due to the difference in local morphology. Namely, high- and low-residual stress regions coexist within YAG and $Al_2O_3$, which accounts for the measured wide distribution of fracture toughness (Fig. 11) and residual stress (Fig. 12) in YAG at least qualitatively.

## 4. Conclusions

The residual stresses at room temperature in YAG of the melt growth $Al_2O_3$/YAG eutectic composite were studied by means of indentation fracture test and finite element analysis. As a reference sample without thermally induced residual stress, the bare YAG taken out from the composite was used. Main results are summarized as follows.

(1) The crack in YAG in the composite tends to by-pass $Al_2O_3$, while the crack in $Al_2O_3$ tends to run into YAG, suggesting that the residual stresses are compressive and tensile in YAG and $Al_2O_3$, respectively.
(2) The indentation fracture test showed that the fracture toughness of YAG in the composite was higher than that of the bare YAG taken out from the composite. From the difference in fracture toughness value, the residual stress of YAG in composite was estimated to be around $-170 \pm 100$ and $-220 \pm 130$ MPa for Faces A and B, respectively.
(3) The fracture toughness and therefore the residual stress of YAG in composite were different from position to position, depending on the local morphology. The residual stresses of YAG, estimated by the indentation fracture test, were in the ranges of around −400 to 0 MPa and around −500 to 0 MPa for Faces A and B, respectively.
(4) The average residual stresses in YAG in composite calculated by the finite element analysis were −150 and −180 MPa in Faces A and B, respectively. The residual stresses of YAG, calculated by the FEM, were in the range of around −300 to 0 MPa in Faces A and B. These calcu-

lation results were comparable to the experimental results mentioned in (2) and (3) above.

(5) The experimentally observed wide distribution of residual stress in YAG (and $Al_2O_3$) was accounted for by the difference in local morphology based on the result of the finite element analysis.

## References


[1]. Mazerolles, L., Michel, D. and Protier, R., Microstructure and mechanical behavior of $Al_2O_3$–$ZrO_2(Y_2O_3)$. *J. Phys.*, 1986, **47**(C-1), 335–339.

[2]. Waku, Y., Nakagawa, N., Otsubo, H., Shimizu, K. and Kohtoku, Y., A ductile ceramic eutectic composite with high strength at 1873 K. *Nature*, 1997, **389**, 49–52.

[3]. Waku, Y., Nakagawa, N., Wakamoto, T., Otsubo, H., Shimizu, K. and Kohtoku, Y., High temperature strength and thermal stability of unidirectionally solidified $Al_2O_3$/YAG eutectic composite. *J. Mater. Sci.*, 1998, **33**, 1217–1224.

[4]. Yang, M., Jeng, S. M. and Chang, S. Y., Fracture behavior of directionally solidified $Y_3Al_{15}O_{12}/Al_2O_3$ eutectic fiber. *J. Am. Ceram. Soc.*, 1996, **79**, 1218–1222.

[5]. Sayir, A. and Framer, S. C., The effect of the microstructure on mechanical properties of directionally solidified $Al_2O_3$–$ZrO_2(Y_2O_3)$ eutectic. *Acta Mater.*, 2000, **48**, 4691–4697.

[6]. Pastror, J. Y., Poza, P., Llorca, J., Pena, J. I., Merino, R. I. and Orera, V. M., Mechanical properties of directionally solidified $Al_2O_3$–$ZrO_2(Y_2O_3)$ eutectics. *Mater. Sci. Eng. A*, 2001, **308**, 241–249.

[7]. Yoshida, H., Nakamura, A., Sakuma, T., Nakagawa, N. and Waku, Y., Anisotropy in high-temperature deformation in unidirectionally solidified eutectic $Al_2O_3$–YAG single crystals. *Scripta Mater.*, 2001, **45**, 957–963.

[8]. Ochiai, S., Ueda, T., Sato, K., Hojo, M., Waku, Y., Nakagawa, N., Sakata, S., Mitani, A. and Takahashi, T., Deformation and fracture behavior of $Al_2O_3$/YAG composite from room temperature to 2023 K. *Compos. Sci. Technol.*, 2001, **61**, 2117–2128.

[9]. Fernadez, J. M., Sayir, A. and Framer, S. C., High temperature creep deformation of directionally solidified $Al_2O_3/Er_3Al_5O_{12}$. *Acta Mater.*, 2003, **51**, 1705–1720.

[10]. Harada, H., Suzuki, T., Hirano, K. and Waku, Y., Ultra-high temperature compressive creep behavior of an in-situ $Al_2O_3$ single-crystal/YAG eutectic composite. *J. Eur. Ceram. Soc.*, 2004, **24**, 2215–2222.

[11]. Matson, L. E. and Hecht, N., Creep of directionally solidified alumina/YAG eutectic monofilaments. *J. Eur. Ceram. Soc.*, 2005, **25**, 1225–1239.

[12]. Ochiai, S., Sakai, Y., Sato, K., Tanaka, M., Hojo, M., Okuda, H., Waku, Y., Nakagawa, N., Sakata, S., Mitani, A. and Takahashi, T., Fracture characteristics of $Al_2O_3$/YAG composite at room temperature to 2023 K. *J. Eur. Ceram. Soc.*, 2005, **25**, 1241–1249.

[13]. Hirano, K., Application of eutectic composites to gas turbine system and fundamental fracture properties up to 1700 °C. *J. Eur. Ceram. Soc.*, 2005, **25**, 1191–1199.

[14]. Nakagawa, N., Ohtsubo, H., Mitani, A., Shimizu, K. and Waku, Y., High temperature strength and thermal stability for melt growth composite. *J. Eur. Ceram. Soc.*, 2005, **25**, 1251–1257.

[15]. Llorca, J. and Orera, V. M., Directionally solidified eutectic ceramic oxides. *Prog. Mater. Sci.*, 2006, **51**, 711–808.

[16]. Ochiai, S., Ueda, T., Sato, K., Hojo, M., Waku, Y., Sakata, S., Mitani, A., Takahashi, T. and Nakagawa, N., *Elastic Modulus and Coefficient of Thermal Expansion of Al2O3/YAG Composite at Ultra High Temperatures. Mater. Sci. Res. Int.* Special Technical Publication-2. The Society of Materials Science, Kyoto, Japan, 2001, pp. 282–285.

[17]. Dickey, E. C., Frazer, C. S., Watkins, T. R. and Hubbard, C. R., Residual stresses in high-temperature ceramic eutectics. *J. Eur. Ceram. Soc.*, 1999, **19**, 2503–2509.

[18]. Torii, S., Kamiyama, T., Oikawa, K., Waku, Y. and Fukunaga, T., Strain measurement of the directionally solidified eutectic $Al_2O_3/Y_3Al_5O_{12}$ (YAG) ceramic by neutron diffraction. *J. Eur. Ceram. Soc.*, 2005, **25**, 1307–1311.

[19]. Sha, J. J., Ochiai, S., Okuda, H., Waku, Y., Nakagawa, N., Mitani, A., Sato, M. and Ishikawa, T., *Residual Stresses in YAG Phase of Directionally Solidified $Al_2O_3$/YAG Eutectic Ceramic Composite Estimated by X-ray Diffraction. J. Eur. Ceram. Soc.* [submitted as the 2nd DSEC workshop paper].

[20]. Evans, A. and Charles, E. A., Fracture toughness determination by indentation. *J. Am. Ceram. Soc.*, 1976, **59**, 371–372.

[21]. Niihara, K., Morena, R. and Hasselman, D. P. H., Evaluation of $K_{Ic}$ of brittle solids by the indentation method with low crack-to-indent ratios. *J. Mater. Sci. Lett.*, 1982, **1**, 13–16.

[22]. Marshall, D. B. and Lawn, B. R., An indentation technique for measuring stresses in tempered glass surfaces. *J. Am. Ceram. Soc.*, 1977, **60**, 86–87.

[23]. Iost, A. and Foct, J., Toughness and residual stresses in galvanizing coatings. *J. Mater. Sci.*, 1993, **12**, 1340–1343.

[24]. Simmons, G. and Wang, H., *Single Crystal Elastic Constants and Calculated Aggregate Properties; A Handbook*. M.I.T. Press, Massachusetts, 1971, p. 328.

[25]. Alton, W. J. and Barlow, A. J., Temperature dependence of the elastic constants of yttrium aluminum garnet. *J. Appl. Phys.*, 1967, **38**, 3023–3024.

[26]. Touloukian, Y. S., Kirby, R. K., Taylor, R. E. and Lee, T. Y. R., *Thermophysical Properties of Matter, Vol. 13, Thermal Expansion, Nonmetallic Solids*. Plenum, New York, 1977, pp. 176–193.

[27]. Gupta, T. K. and Valentich, J., Thermal expansion of yttrium aluminum garnet. *J. Am. Ceram. Soc.*, 1971, **54**, 335–336.

[28]. Cribb, J. L., Shrinkage and thermal expansion of a two phase material. *Nature*, 1968, **220**, 576–577.

[29]. Waynant, R. and Ediger, M., *Electro-Optics Handbook*. Mcgraw-Hill Inc., New York, 1994, pp. 11.13–11.23.

[30]. Lawn, B. and Wilshaw, R., Indentation fracture: principles and applications. *J. Mater. Sci.*, 1975, **10**, 1049–1081.